SAND2008-1203C

Validation Experiments to Determine Radiation Partitioning of Heat Flux to an Object in a Fully Turbulent Fire

Thomas Blanchat,[1] Tim O'Hern,[2] Sean Kearney,[2] Allen Ricks,[1] and Dann Jernigan[1]
[1]Fire and Aerosol Sciences
[2]Thermal/Fluid Experimental Sciences
Sandia National Laboratories*
P.O. Box 5800
Albuquerque, New Mexico 87185-1135, USA

Submitted to the 32nd Symposium (International) on Combustion
Montreal, Canada
August 3-8, 2008

Corresponding Author: Thomas Blanchat
Sandia National Laboratories
P.O. Box 5800; Mail Stop 1135
Albuquerque, NM 87185 USA
Voice: +1-505-845-3048
Email: tkblanc@sandia.gov
Fax: +1-505-845-3151

Colloquium: Fire Research

Alternate Colloquium: Diagnostics

Total Length: 5800 words determined using Method 1

Word Equivalent Lengths:
Main Text: 3699
Equations: 46
References: 385
Figures: 1670

(Figure 1: 126, Figure 2: 112, Figure 3: 141, Figure 4: 145, Figure 5: 129, Figure 6: 466, Figure 7: 119, Figure 8: 137, Figure 9: 156, Figure 10: 139)

Author agrees to pay color page charges.

* Sandia is a multiprogram laboratory operated by Sandia Corporation, a Lockheed Martin Company, for the United States Department of Energy's National Nuclear Security Administration under Contract DE-AC04-94AL85000.

Abstract

An experimental study was performed to determine the fraction of the heat flux that is due to radiation (sometimes referred to as radiation partitioning of the total heat flux measurement) to a calorimeter engulfed in a large methanol pool fire to improve understanding and develop high-quality data for the validation of fire models. Diagnostics employed include Coherent Anti-Stokes Raman Spectroscopy (CARS), Particle Image Velocimetry (PIV), total and radiative thermometry, and thermocouples. Data are presented not only for the physics measurements but also for all initial and boundary conditions required as necessary inputs to computation models. The large physical scale, the experimental design (enhanced convection relative to radiation heat transfer), the use of independent measurement techniques, and the attention to data quality, provide a unique dataset that emphasizes the convective component to support numerical fire model validation for convective and radiative heat transfer in fires.

Keywords: Pool Fires, Heat Flux, Radiation Partitioning, PIV, CARS

Introduction

The cylinder is one of the canonical geometries for heat transfer, and is a relevant geometry to study the heat flux incident to an object located within the fire plume for the validation of fire models and thermal response codes. A cylindrical calorimeter with sufficient instrumentation to allow direct measurement of heat fluxes was designed, fabricated, and deployed in 2 m diameter methanol pool fires. Data taken during each test included measurement of the incident total and incident radiative heat flux to the calorimeter, the temperatures and velocities of the convective flow near the calorimeter, and the thermal response of the calorimeter in a fully turbulent fire.

Validation quality fire tests are of fundamental interest for heat transfer studies and are commonly used in "abnormal thermal environments" experiments for high-consequence hardware qualification at Sandia National Laboratories. Validation experiments are a special class of experiment in that they are specifically designed for direct comparison with computational predictions [1]. Making meaningful comparisons between the computational and experimental results requires careful characterization and control of the experimental features or parameters used as inputs into the computational model. Validation experiments must be designed to capture the essential physical phenomena, including all relevant initial and boundary conditions.

Ultimately the lower bound of uncertainty for fire model prediction is based on experimental uncertainty. Thus it is important to achieve as low of uncertainty as possible within the harsh measurement environment of a fire. The goal of the current study is to obtain separate estimates of the radiation and convection for a large turbulent methanol fire. Methanol is used both to permit laser-based diagnostics and to enhance the relative contribution of convection. For methanol, the thermal radiation is from gas band emission (H_2O and CO_2), and is not as large (relative to the convection heat transfer) as

for most hydrocarbon fuels. The placement of the calorimeter off-axis so that one side is engulfed and the other is intermittently exposed also permits the variation of convection to radiation within a single experimental data set.

The determination of the fraction of the heat flux that is due to radiation has been reported in the literature by Bryant, et al. [2], Robertson and Ohlemiller [3], and Wetterlund and Persson [4], with measurement uncertainties estimated between 7 and 25% under the conditions of the experiments. For typical large hydrocarbon pool fires, Nakos and Keltner [5] determined that radiation accounts for 80-90% of the heat transfer, thereby swamping the convection heat transfer and making it difficult to ascertain how well the code is actually modeling this phenomenon. Uncertainties are application-dependent and the majority of the data are at small scale (<1 m) and/or do not meet the high standards required for validation (i.e., unknown/uncontrolled boundary conditions and uncertainty).

The experimental apparatus and diagnostics will be described in the next section. This will be followed by a discussion of results with emphasis on experimental uncertainties. The final section will offer concluding remarks.

Experiment Description

The FRH Test Cell

The FLAME/Radiant Heat (FRH) test cell is part of the new Thermal Test Complex (TTC) at Sandia National Laboratories (SNL). Figure 1 shows the FRH facility with a pool fire at the ground level, pipes supplying air flow through the basement, the chimney, and instrumentation rooms outside the FRH chamber. The main test chamber of the FRH cell is cylindrical in shape (18.3 m inner diameter) with a

height around the perimeter of 12.2 m. The ceiling slopes upwards (~18º) from the perimeter walls to a height of 14.6 m over the center of the facility. A round hole at the top of the facility (4.9 m diameter) transitions to a 3.0 m by 3.7 m chimney duct. The outer walls are made of steel channel sections and are filled with water to maintain a relatively constant wall temperature during tests. The ground level of FRH can be divided into three concentric sections; a liquid fuel (JP8, methanol, etc.) pan or gas (H_2, methane, He, etc.) burner (up to 3 m in diameter), spill plates, and grating for inlet combustion air. Air enters the FRH cell via the 3.05 m diameter pipe and is distributed by 18 supply pipes to an annulus along the subbasement circumference. Air entering the chamber ground level was characterized experimentally and shown to be uniform within 10% of the mean flow.

The Cylindrical Calorimeter

Heat flux to the calorimeter surface was measured using two different measurement techniques, in accordance with the guiding principles of validation experiments. The first technique used thermocouples (TCs) attached to the calorimeter to compute incident heat flux using a 1-D inverse heat conduction methodology. In the method, the TC temperature history is used to estimate absorbed (combined radiative and convective) heat flux using known boundary conditions, material properties and dimensions. One can add a term approximating the energy reradiated to obtain a measure of the total incident heat flux. The commercial software used to estimate the heat flux from the temperature measurements is IHCP1D© (Beck Engineering Consultants Company).

The second technique used commercial thermopile heat flux gauges (HFGs). Each HFG contained both a total thermopile (180º view angle) and a gas purged, window shielded thermopile (radiometer,

150º view angle). The combination of these two thermopiles on one gauge allowed direct measurement of the incident total and radiative heat fluxes, from which the convective heat flux may be determined by differencing the two.

The cylindrical calorimeter had a center section 0.46 m in length, within which all of the sensors are mounted, and two end sections of length 0.76 m each. All three sections were made of 304 stainless steel (3 mm thick, 0.30 m OD). A steel pipe (50 mm OD) down the center of the calorimeter formed the backbone of the structure, and the outer shells were held in place by four center supports in the shape of an eight-pointed star. Steel end caps (13 mm thick) completed the structure of the calorimeter. The inside center section of the calorimeter was filled with a ceramic fiber blanket insulation (Durablanket® S type, rated to 1260ºC, 128 kg/m^3 density). The outer surface of the center section of the cylindrical calorimeter was painted with high-temperature, high-emissivity Pyromark® 2500 paint.

A total of 36 thermocouples (TCs) (1.0 mm, type-K) were attached to the inside of the outer shell of the center section, located on a uniform 5 × 8 grid. The grid spacing in the axial direction is 76 mm between TC locations, and the angular spacing is 45º about the axis of the calorimeter. Four grid locations at the axial midpoint of the cylindrical calorimeter were occupied with HFGs in place of TCs (Schmidt-Boelter Medtherm® (MT) Model 96-15T-15RP(ZnSe)-21745 dual-mode). Sensor MT1 faced down, MT2 faced the fire and the CARS volume (discussed later) at pool centerline, MT3 faced up, and MT4 faced away from pool centerline. The gauges were operated at constant temperature (50°C) to prevent the formation of fuel condensation. The required lines and hoses for the water cooling and gas purging, along with electrical wiring for the TCs and HFGs, were routed inside the calorimeter to the calorimeter endplates. Figure 2 shows the inside of the calorimeter, with insulation, plumbing, and TCs mounted to the inner surface of the calorimeter outer shell. Note the four HFG locations visible at the midplane.

Figure 3 shows the calorimeter placed 0.94 m above the liquid pool surface, centered on the longitudinal axis and with a radial offset (10.2 cm from pool centerline to the calorimeter edge). The white insulation-wrapped split pipe in the foreground was used to propagate the laser beams used for the CARS gas temperature measurements.

CARS and PIV Measurements

Additional instrumentation fielded in the 2-m-diameter methanol pool-fire utilized two modern laser-diagnostic approaches, PIV and CARS thermometry. PIV-derived free-stream gas velocity, combined with the gas temperature outside the boundary layer from CARS and the surface temperature on the calorimeter, were used to estimate of the convective heat transfer.

CARS provides a point measurement of gas temperatures by a noninvasive, laser-based probing of the reacting flow field [6-7]. Three pulsed laser beams were propagated into the FRH cell and focused at pool centerline (~10 cm from the face of MT2) to form a CARS probe volume just outside of the thermal boundary layer of the cylindrical calorimeter. The CARS signal beam was forward propagated and fiber coupled to a remotely located high-resolution grating-based spectrograph. The spectral content of the CARS signal captured on a CCD camera revealed how nitrogen population within the CARS probe volume was distributed among the allowed rotational and vibrational states and the gas temperature was determined from a best fit of theory to the experimentally obtained spectra. Figure 4 shows a time-exposed photograph of the 2-m diameter methanol pool fire (without calorimeter) with the light pipes used to propagate the CARS-instrument laser beams. The green, orange and yellow colors arise from stray reflections and scattering of the CARS laser beams.

A PIV experiment typically involves seeding the flow field of interest with flow-following seed particles, then acquiring images of the laser-illuminated particle field in two or more consecutive images. The images are separated by a short time period that is determined by the flow speed since the particle field from the first image needs to be identifiable in the second image [8-9]. Analysis by cross-correlation yields velocity vectors. Most applications of PIV are at a laboratory scale, and applications to fires are limited. At Sandia National Laboratories, we have applied PIV for measurements in 1 m diameter helium plumes and methane and hydrogen fires [10-13]. That work was done using ultraviolet excimer lasers and film cameras, which caused some obvious difficulties in turnaround time and the ability to optimize the PIV seeding, illumination, etc. The present work implemented a simpler, more robust PIV system, using visible Nd:YAG lasers and digital cameras to measure the velocity field just outside the boundary layer on the cylindrical calorimeter in order to characterize the convective heat transfer environment.

The PIV lasers were Continuum Surelite Nd:YAG lasers, frequency doubled to 532 nm. They produce approximately 8 ns pulses with a pulse energy of 400 mJ at a 10 Hz pulse repetition rate. The laser beam was converted to a light sheet by a combination of a 4.957 m spherical lens and a 150 mm cylindrical lens. At the measurement location, 7.3 m from the cylindrical lens, the sheet was about 38 cm high and 1 mm thick. Spatially-calibrated images of particle motion in the fire were captured with a Photometrics CoolSnap Diff HQ camera with an AF Micro Nikkor lens (105 mm, f/22). A 532 nm interference filter with 3 nm full width half max was used to pass only laser light to the camera (~4.3 m distant), blocking most of the fire emission.

Seeding fires is difficult due to the gas volumetric expansion as the fuel is combusted. Seeding levels that would provide adequate tracers in an isothermal gas flow yield very dilute seeding when the hot combustion gases expand. The choice of particles and seeding techniques was based on previous

experience with PIV in fires [12-13]. A mixture of glass microballoons (3M Scotchlite K1, 65 micron mean diameter, density 0.125 g/cc) and ceramic particles (mixes of 3M G-200, G-200PC, G-400, W-210, or W-410, all 3-5 micron mean diameter, density 2.4 g/cc) were used. The seeders were fabricated from stainless steel tubes (19 mm diameter) with a milled long slit that was covered with a fine 20 mesh stainless steel screen. Immediately prior to each run the seed tubes were filled with the particle mixture and suspended above the fuel pan on either side of the laser light sheet, with the screens facing downward. At the desired time during the fire, seeding was initiated by energizing electronic vibrating motors attached to the tubes. Figure 5 shows the seeders installed and operating during a PIV run. The blue color visible just above the liquid surface is gas band radiation from the methanol fire. The green color coming in from the right and striking the calorimeter on the left is due to scattering of Nd:YAG laser light by the PIV seed particles and seeders. The yellow and red are the thermal emission of the seed particles entrained in the flame sheets of the methanol fire (acting like artificial soot). Cross-correlation PIV analysis was performed using PIV Sleuth [14].

Fuel Regression

Burning (mass loss) rate for the liquid methanol pool fires was determined by measuring the transient liquid pool head pressure (two 0-64 mm water column Rosemount Model 3051 differential pressure gauges).

Data Acquisition and Uncertainty

Data acquisition (DAQ) was PC-based using 16-bit National Instruments (NI) data acquisition hardware. Thermocouple and heat-flux data were sampled simultaneously for all channels, typically at 1000 Hz with an average value recorded at a rate of at least one sample per second. Channel integrity was evaluated prior to each experiment with a calibrated voltage source. All thermocouple channels had an uncertainty to within ±1.7 K. The uncertainty of the entire DAQ (and associated instrumentation) was estimated by assessing the individual uncertainties of each component, then combining them using the root-sum-square (RSS) method [15].

Results

Twenty methanol fire experiments were performed. Only the HFG results from the first nine experiments are presented. The later experiments mainly concentrated on obtaining PIV and CARS data; PIV seed deposition and thermal insult from sequential fires yielded unreliable HFG results for those datasets. Average initial and boundary conditions include: 1) 21±3°C wall temperature, 2) 19±3°C liquid fuel and ambient air temperature, 3) 0.82±0.01 atm ambient air pressure, and 4) 1.11±0.08 mm/min fuel regression rate with a corresponding mass flux of 0.015 kg/m^{2}s. The forced draft fan provided ~58 standard m^3/s of air into the cell. Steady-state fire durations were in the range of 10-30 minutes.

A 2 m diameter methanol fire is fully turbulent. Analysis of video yielded a median flame height of 2 m. In addition, the fire plume ‘necked in’ close to the fuel surface and was <1 m in width at the calorimeter. Due to the off-centerline position, during each puff cycle the fire curled under the

calorimeter to briefly expose gauge MT4, which faced toward the cold FRH wall and away from the fire plume. Figure 6 shows larger total time-averaged heat fluxes measured at MT1 (facing down) and MT2 (facing the fire plume) compared to MT3 and MT4 for each experiment. The average steady-state flux from the nine experiments and a one standard deviation bound on the average (experiment series variability) is also shown (the solid lines with the uncertainty bound). The relative contribution of the convective heat flux to the total flux is also shown in Figure 6. MT1-MT3 had approximately a 60%/40% partitioning of the heat flux into radiative and convective contributions. MT4 (facing away from the fire), had a 25%/75% partitioning of the flux.

Figure 7 presents a comparison of the MT flux (both total and radiative) to that computed using inverse heat conduction (TC6 flux, located 7.6 cm from the MT1 thermopile). Note that initially the TC flux matches the total MT (water-cooled) flux but as the calorimeter heats (TC6 temperature in Figure 7) reducing the convection the TC flux trends to the MT radiative flux measurement. The fluxes are highly fluctuating and for clarity are plotted using a 30 s running average. Figueroa et al. [16] estimated the maximum uncertainty in heat flux using the inverse heat conduction program IHCP1D© to be about ±20% for a cylindrical calorimeter near, but not in, a fire. Nakos [17] showed that the incident flux uncertainty could be as large as ±40% in situations broadly similar to those of the present experiments.

Figure 8 shows the 1-minute average thermocouple flux at the eight radial positions at the start of experiment 1 and compares that to the same 1-minute average total heat flux by thermopile (shown with a 12% uncertainty bound). The asymmetry of the flux caused by the location of the calorimeter (off pool centerline) is clearly evident. A slight tilting of the fire is also evident, as indicated by a preferential shift of the TC-determined flux to one side of the calorimeter.

Thermopile Uncertainty

All uncertainty reported below are expressed as a percentage of the measured value. Measurement uncertainty of the net flux for both the total and the radiative-only thermopiles, per the manufacturer, is ±3% of the measurement across the calibration range of 0 to 150 kW/m^2. This uncertainty, however, is based on a calibration methodology which uses only a radiative heat source and does not adequately account for the additional uncertainty introduced by the uncertain gauge temperature and emissivity.

For the radiometer, the composite uncertainty in the incident radiative flux is ±11% over the range of expected heat fluxes. This is based on the methodology prescribed by Nakos [17] and using an uncertainty of ±10% for the radiometer gauge emissivity and the gauge surface temperature (assumed equal to the gauge cooling water temperature).

A set of convection calibrations on four representative Schmidt-Boelter gages demonstrated the effects of convective heat flux on the sensitivity of the total heat flux gages [T. Diller, Virginia Tech University unpublished report, 2007]. In all cases the output decreased in proportion to the convective heat transfer coefficient (h). The effect is for the gage to read a smaller heat flux (about 2%) when h is ~10 W/m^2-K (typical for buoyancy-driven fires). The measurement uncertainty in the corrected net heat flux (assuming ±50% uncertainty in h) is approximately ±3.5% over the range of conditions expected in the experiments. As in the radiative flux case, the conversion from net to incident flux introduces additional uncertainties due to the uncertain emissivity and surface temperature. If the convective fraction is assumed to be known to within ±0.25, the uncertainty in the total incident heat flux is ±12%.

The uncertainty in the convective flux can be quite large when convection is small relative to radiation. With uncertainties in incident fluxes assumed to be ±11% for the radiative and ±12% for the

total, the uncertainty in the convective flux is ±43% when the radiative fraction is 0.67 and ±16% when the radiative fraction is 0.25, corresponding to the range of experimentally-observed values.

The uncertainty in the radiative fraction can be determined from the uncertainties in the incident radiative and incident total heat fluxes. With uncertainties as assumed in the convection heat flux calculations, the uncertainty in the radiative fraction is ±16%. This corresponds to uncertainties in the convective fraction of ±33% when the radiative fraction is 0.67 and ±5% when the radiative fraction is 0.25.

Summarizing, the uncertainty in the incident radiative flux is ±11%, uncertainty in the total incident flux is ±12%, and uncertainty in the convective heat flux will generally fall between ±16% and ±43% for the present experiment.

Convective heat flux estimates using PIV and CARS

The convective heat transfer coefficient can be estimated from the velocity and the temperature of the gas free-stream by means of an appropriate empirical correlation. Figure 9 (a compilation averaging 1000 cross-correlated images, with the number of vectors shown reduced for clarity) shows that at the CARS measurement volume location, the average horizontal and vertical velocity was 0.5 and 1.8 m/s, respectively.

Figure 10 shows a histogram obtained from 390 single-shot CARS temperature measurements with the calorimeter in-place, resulting in an average gas temperature of 1083 K, and a large standard deviation of 419 K, which is to be expected given the highly fluctuating (i.e., ~1 Hz puff frequency) environment observed during the experiments.

The experimentally determined *local* convective heat-transfer coefficient, h_{exp}, on the cylinder surface at sensor MT2 was determined (Eqn. 1) from the measured convective flux, q''_{conv}, of 12.1±4.5 kW/m^2 in conjunction with a gauge surface temperature, T_s (323 K) and average CARS-measured gas temperature, T_∞ (1083 K)

$$h_{exp} = \frac{q''_{conv}}{(T_s - T_\infty)} \qquad (1)$$

to obtain a measured value of ~16 W/m^2-K. This is consistent with the expected order of magnitude of gas-phase convection coefficients. This measurement is compared to an engineering estimate of the convective heat-transfer coefficient that was determined assuming flow over a cylinder exposed to the velocity and temperature conditions in the fire plume. At the average PIV-measured free-stream speed, the local Reynolds number, Re_D is of order 8000, such that the boundary layer flow on the calorimeter surface is laminar. The Hilpert [18] correlation (Eqn. 2) with constants C = 0.193, m = 0.618,

$$\overline{Nu}_D = \frac{\overline{h}\, D}{k} = C\, Re_D^m Pr^{1/3} \qquad (2)$$

is used to obtain an estimate of the *average* heat-transfer coefficient, h, where D is the calorimeter diameter and the thermophysical properties of the gas (assumed dry air) are evaluated at the film-temperature average (703 K) of the surface and fire-gas temperatures. With this approach, an engineering estimate of h = ~8 W/m^2-K for the *surface-averaged* heat-transfer coefficient is obtained, which is within a factor of two of our measured *local* value. Note that the cylinder is not really

immersed in a cross flow of constant velocity; therefore, the boundary layer development is not quite the same as cylinder in cross flow. Also, other factors, such as flow separation near the MT2 90° location [18] and free-stream turbulence [19] can cause large variations in $\overline{h}$ or $\overline{Nu}_D$.

Concluding Remarks

Detailed measurements related to the partitioning of heat flux to an object in large-scale fully-turbulent methanol fires have been taken for the purpose of model validation. Care has been taken in the design of experiments to ensure that convection is an important component and varies in importance such that the data can be used to evaluate the uncertainty in numerical model prediction of both radiation and convection. Using methanol also eliminates soot as the primary radiative source, thus providing a data set that is based on gas band radiation only. Since the work is primarily designed to provide validation, it follows the recommendations for the design of validation-quality datasets including the measurement (with estimation of all experimental uncertainty) of all initial and boundary conditions required as numerical simulation input. The data sets (available on request) are unique in the first use of CARS, PIV, thermopiles, and thermocouples in the same experiment and conducted in a new large-scale fire research laboratory specifically designed to provide validation quality data. Future work will focus on extending the CARS and PIV measurements.

References

1. Trucano, T. G., Pilch, M., and Oberkampf, W. L., Sandia Report SAND2002-0341.

2. Bryant, R., Womeldorf, C., Johnsson, E., and Ohlemiller, T., *Fire and Materials*, 27:209-222, (2003).

3. Robertson, A. F., and Ohlemiller, T. J., *Fire Safety Journal*, 25:109-124 (1995).

4. Wetterlund, I., and Persson, B., *Calibration and use of heat flux meters*, 1:35, Interscience Communications Ltd., London, England, 1999.

5. Nakos, J. T., and Keltner, N. R., *Heat Transfer in Radiation, Combustion and Fires*, 106-2:381-388 (1989).

6. Kearney, S. P., and Grasser, T. W., AIAA-2007-872, Reno, 2007.

7. Kearney, S. P., and Jackson, M. N., "Dual-Pump Coherent Anti-Stokes Raman Scattering Thermometry in Heavily Sooting Flames," *AIAA Journal*, accepted for publication, 2007.

8. R. J. Adrian, *Experiments in Fluids* 39:159-169 (2005).

9. Raffel, C. Willert, and J. Kompenhans, *Particle Image Velocimetry: A Practical Guide,* Springer, 2002.

10. O'Hern, T. J. , Weckman, E. J., Gerhart, A. L., Tieszen, S. R., and Schefer, R. W., *Journal of Fluid Mechanics* 544:143-171 (2005).

11. DesJardin, P. E., O'Hern, T. J., and Tieszen, S. R., *Physics of Fluids* 16:1866-1883 (2004).

12. Tieszen, S. R., O'Hern, T. J., Schefer, R. W., Weckman, E. J., and Blanchat, T. K., *Combustion and Flame* 129:378-391 (2002).

13. Tieszen, S. R., O'Hern, T. J., Weckman, E. J., and Schefer, R. W., *Combustion and Flame* 129:378-391 (2004).

14. Christensen, K. T., Soloff, S. M., and Adrian, R. J., *PIV Sleuth – Integrated Particle Image Velocimetry Interrogation/Validation Software,* Department of Theoretical and Applied Mechanics Report 943, University of Illinois at Urbana-Champaign, 2000.

15. Coleman and Steele, *Experimentation and Uncertainty Analysis for Engineers*, Wiley & Sons, 1999.

16. Figueroa, V. A., Nakos, J. T., and Murphy, J. E., Sandia Report SAND2005-0339.

17. Nakos, J. T., Sandia Report SAND2005-7144.

18. Incropera, F. P., and DeWitt, D. P., *Fundamentals of Heat and Mass Transfer*, 4th edition, Wiley & Sons, 1996.

19. Szczepanik, K., Ooi, A., Aye, L. and Rosengarten, G., 15th Australasian Fluid Mechanics Conference, The University of Sydney, Sydney, Australia, December 2004.

20. Kest, J., Advances in Heat Transfer, Vol. 3, Academic Press, NY, 1966.

List of Figures

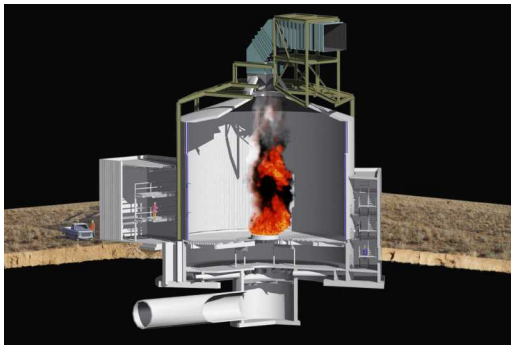

Fig. 1. The FRH facility.

Fig. 2. Inside the cylindrical calorimeter.

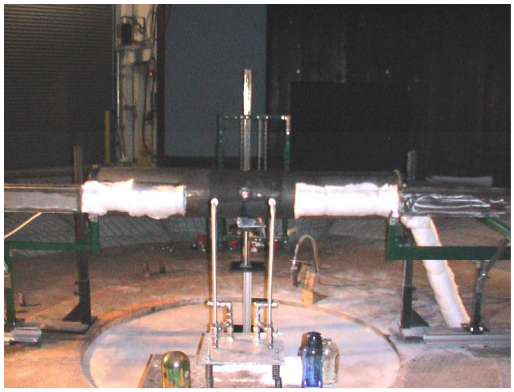

Fig. 3. Location of calorimeter and HFGs.

Fig. 4. CARS measurement.

Fig. 5. PIV measurement.

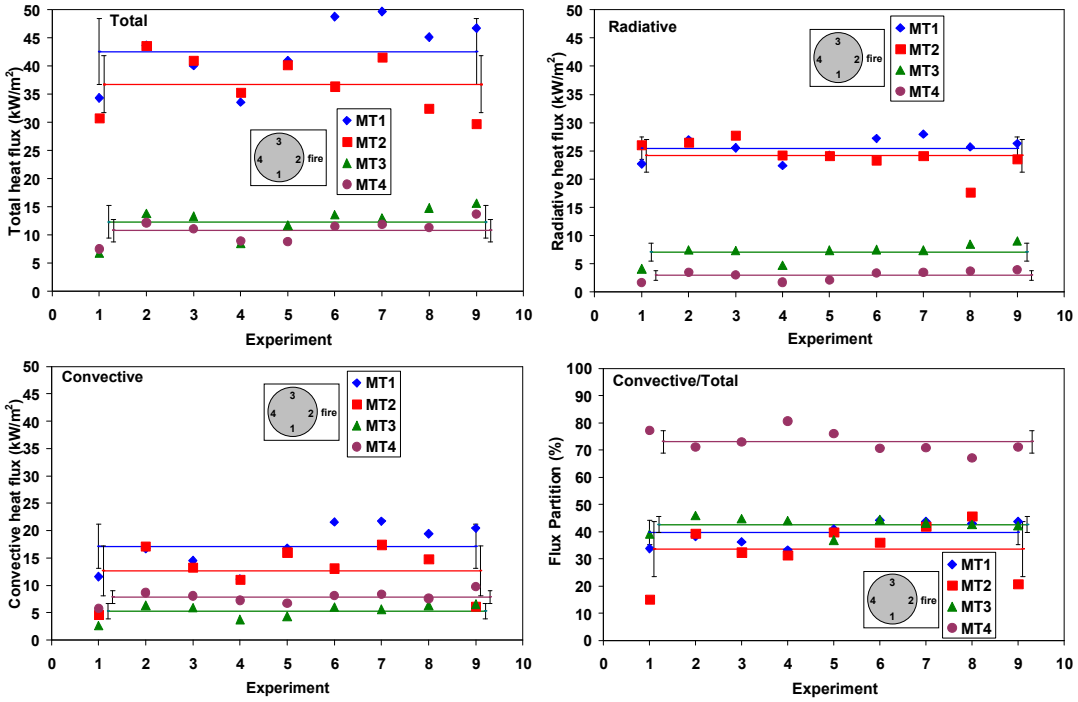

Fig. 6. Time-averaged heat fluxes by location.

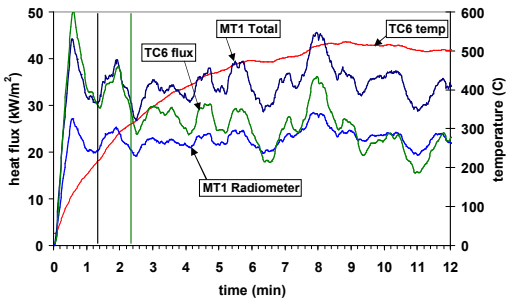

Fig. 7. Thermopile to TC flux comparison.

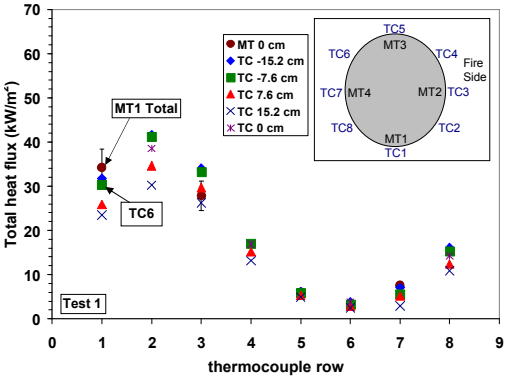

Fig. 8. Asymmetric circumferential flux.

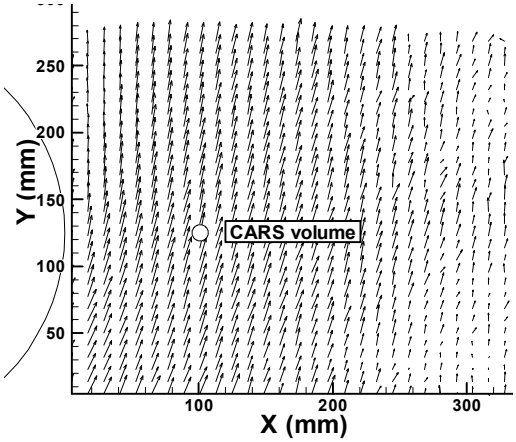

Fig. 9. PIV determined gas velocity.

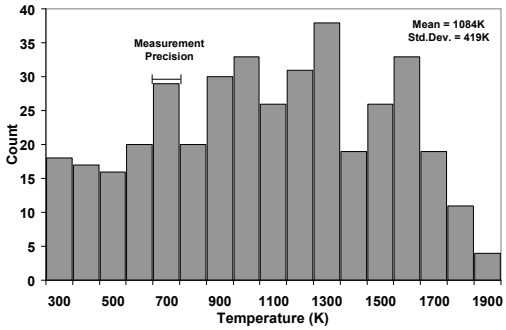

Fig.10. CARS temperature histogram.